JP Journal of Heat and Mass Transfer

https://pphmjopenaccess.com
https://doi.org/10.17654/0973576324042
Volume 37, Number 5, 2024, Pages 667-684 **P-ISSN: 0973-5763**

FLOW OF EYRING-POWELL HYBRID NANOFLUID ON A SHRINKING CYLINDER WITH JOULE HEATING AND VISCOUS DISSIPATION

Iskandar Waini*, Umair Khan, Aurang Zaib, Anuar Ishak and Ioan Pop

Fakulti Teknologi dan Kejuruteraan Industri dan Pembuatan
Universiti Teknikal Malaysia Melaka
Hang Tuah Jaya, 76100 Durian Tunggal, Melaka
Malaysia
e-mail: iskandarwaini@utem.edu.my

Department of Mathematics and Social Sciences
Sukkur IBA University
Sukkur 65200, Sindh, Pakistan

Department of Mathematical Sciences
Federal Urdu University of Arts, Science and Technology
Gulshan-e-Iqbal Karachi-75300, Pakistan

Received: July 25, 2024; Revised: August 15, 2024; Accepted: August 27, 2024
Keywords and phrases: dual solutions, Eyring-Powell hybrid nanofluid, shrinking cylinder, viscous dissipation.
*Corresponding author
Communicated by Eugenia Rossi di Schio

How to cite this article: Iskandar Waini, Umair Khan, Aurang Zaib, Anuar Ishak and Ioan Pop, Flow of Eyring-Powell hybrid nanofluid on a shrinking cylinder with Joule heating and viscous dissipation, JP Journal of Heat and Mass Transfer 37(5) (2024), 667-684. https://doi.org/10.17654/0973576324042

Published Online: October 3, 2024

Department of Mathematical Sciences
Faculty of Science and Technology
Universiti Kebangsaan Malaysia
43600 UKM Bangi, Selangor, Malaysia

Department of Mathematics
Babeş-Bolyai University
Cluj-Napoca, 400084, Romania

Abstract

This paper deals with the AA7075-AA7072/methanol hybrid nanofluid flow incorporated with the Eyring-Powell model. The fluid flows over a shrinking cylinder subject to magnetohydrodynamic (MHD), Joule heating, and viscous dissipation. The governing equations are transformed into similarity equations by employing suitable similarity transformations. Then, MATLAB software is used to program the code with the aid of the bvp4c function. The findings prove that the dual solutions are generated for a certain domain of shrinking parameters. Besides, higher values of heat transfer and skin friction are obtained by the imposition of the magnetic and Eyring-Powell fluid parameters. However, the heat transfer is reduced in the presence of viscous dissipation with a higher Eckert number.

1. Introduction

Engineers and scientists often deal with fluids such as water, air, and oils, which are typically considered Newtonian under specific conditions. However, the assumption of Newtonian behavior often proves inadequate, requiring a detailed exploration of non-Newtonian responses that can be complex and progressive. Such situations commonly arise in industries handling chemicals and plastics, as well as in applications involving oil, biological fluids, and mining. Understanding and replicating these non-Newtonian fluid phenomena are crucial for various industrial sectors. Due to their applicability in industrial sectors such as power engineering, food processing, and petroleum production, the study of non-Newtonian fluids

remains a topic of considerable interest among researchers [1]. Among these fluids, Powell-Eyring fluids [2, 3] offer distinct advantages over other models. Several studies [4-6] suggest that this model is highly accurate and dependable in predicting fluid dynamics across varying polymer sizes. Roşca and Pop [7] and Jalil et al. [8] investigated Powell-Eyring fluid flows in a parallel free stream, while Ara et al. [9] and Akbar et al. [10] explored the effects of radiation and magnetohydrodynamic (MHD), respectively. Numerous studies have addressed different aspects of Eyring-Powell fluids, as documented in references [11-14].

In operations involving fibres and extrusion, the boundary layer flow of stretching/shrinking cylinders is critical. The flow through the cylinder is deemed two-dimensional when the radius of the cylinder exceeds the thickness of the boundary layer. A slender cylinder, on the other hand, has a radius that is in the same order as the thickness of the boundary layer. As a result, rather than being two-dimensional, flow across a cylinder can be assumed to be axisymmetric [15]. Wang [16] investigated the heat transfer induced by an evenly stretched cylinder. Further, Ishak et al. [17] studied the flow behavior when the cylinder's surface is permeable. Meanwhile, the studies on shrinking cylinder are reported by Awaludin et al. [18] and Roy and Akter [19].

Choi and Eastman [20] used the term nanofluid to describe a mixture of a base fluid and nanoparticles. Pak and Cho [21] appeared to be the first to develop thermophysical correlations for nanofluids. Ho et al. [22] improved the nanofluid correlations introduced by Pak and Cho [21]. The experimental results contradict the numerical expectations based on existing nanofluid correlations. The dispersion of nanoparticles in the base fluid resulted in a significant reduction rather than an augmentation. As a result, they developed new Al_2O_3-water nanofluid correlations by fitting the experimental results using a least-square curve. In addition, to create a hybrid nanofluid, several types of nanoparticles are disseminated in the base fluid. Takabi and Salehi [23] have presented the new hybrid nanofluid

correlations, which were widely used by various researchers [24-27]. Additionally, Waini et al. [28, 29] reported the temporal stability analysis in hybrid nanofluid flow. Other studies on nanofluid and hybrid nanofluid can be found in references [30-34].

This study aims to explore AA7075-AA7072/methanol hybrid nanofluid incorporated with Eyring-Powell fluid model on the cylinder surface subjected to viscous dissipation and Joule heating effects. It is worth to mention that, this paper examined on the dual solutions and the critical values of the physical parameters which are not yet reported in previous studies. The findings of these studies could supply engineers and researchers with the first clues they need to forecast and regulate the effect of physical parameters in the application area. Jalil et al. [8] justified that the use of the Powell-Eyring fluid model offers a clear advantage over other non-Newtonian fluids because it is based on the kinetic theory of gases and behaves like a viscous fluid at high shear rates. Incorporating this model into the AA7075-AA7072/methanol hybrid nanofluid flow analysis improves the understanding of fluid behavior by considering non-Newtonian effects and the interactions between nanoparticles and the base fluid. Aluminum alloy nanoparticles AA7075 and AA7072 are distinguished as exceptional nanomaterials because of their outstanding thermal, chemical, and physical properties. Their unique characteristics and superior qualities make them highly sought after for numerous industrial applications, particularly in aerospace, in the production of transportation equipment, including glider aircraft and rocket frames.

2. Mathematical Formulation

Figure 1 illustrates the physical model of Eyring-Powell fluid flow towards a shrinking cylinder.

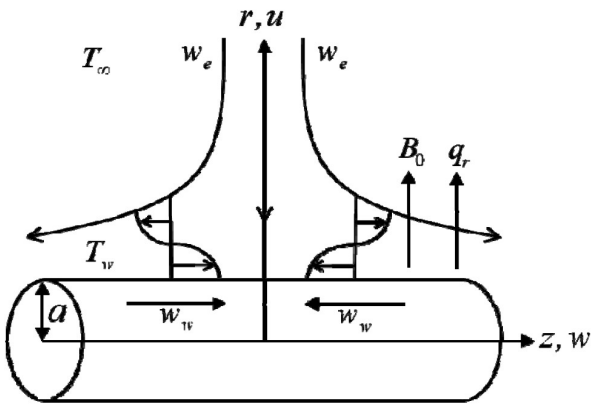

Figure 1. Physical model.

In addition, AA7075-AA7072 nanoparticles were dispersed in methanol to form the hybrid nanofluid. The free stream velocity is $w_e(z) = 2cz$ with $c > 0$ and the surface velocity is denoted by $w_w(z) = 2bz$ with constant b. Moreover, the Joule heating, viscous dissipation, and the radiative heat flux $q_r = -(4\sigma^*/3k^*)(\partial T^4/\partial y)$, where $T^4 \cong 4T_\infty^3 T - 3T_\infty^4$ with σ^* and k^* signifies the Stefan-Boltzmann and the Rosseland mean absorption coefficients [35], are employed in the energy equation. The magnetic field effect B_0 is also considered. Accordingly, the governing equations are [36-39]:

$$\frac{\partial(rw)}{\partial z} + \frac{\partial(ru)}{\partial r} = 0, \tag{1}$$

$$w\frac{\partial w}{\partial z} + u\frac{\partial w}{\partial r} = w_e\frac{dw_e}{dz} + \left(\frac{\mu_{hnf}}{\rho_{hnf}} + \frac{1}{\rho_{hnf}\beta\delta}\right)\left(\frac{\partial^2 w}{\partial r^2} + \frac{1}{r}\frac{\partial w}{\partial r}\right)$$
$$- \frac{1}{6\rho_{hnf}\beta\delta^3}\left(3\left(\frac{\partial w}{\partial r}\right)^2\frac{\partial^2 w}{\partial r^2} + \frac{1}{r}\left(\frac{\partial w}{\partial r}\right)^3\right)$$
$$- \frac{\sigma_{hnf}}{\rho_{hnf}}B_0^2(w - w_e), \tag{2}$$

$$w\frac{\partial T}{\partial z}+u\frac{\partial T}{\partial r}=\left[\frac{k_{hnf}}{(\rho C_p)_{hnf}}+\frac{16\sigma^* T_\infty^3}{3(\rho C_p)_{hnf}k^*}\right]\left(\frac{\partial^2 T}{\partial r^2}+\frac{1}{r}\frac{\partial T}{\partial r}\right)$$
$$+\frac{1}{(\rho C_p)_{hnf}}\left(\left(\mu_{hnf}+\frac{1}{\beta\delta}\right)\left(\frac{\partial w}{\partial r}\right)^2-\frac{1}{6\beta\delta^3}\left(\frac{\partial w}{\partial r}\right)^4\right)$$
$$+\frac{\sigma_{hnf}}{(\rho C_p)_{hnf}}B_0^2(w-w_e)^2 \tag{3}$$

subject to:

$$u=0,\ w=w_w,\ T=T_w \text{ at } r=a,$$
$$w\to w_e,\ T\to T_\infty \text{ as } r\to\infty, \tag{4}$$

where T is the temperature and w and u are the velocity components. Meanwhile, the surface temperature is $T_w(z)=T_\infty+T_0z^2$ with constant T_∞ (ambient temperature) and T_0 (reference temperature). Also, $\beta=\beta_0z^{-1}$ and $\delta=\delta_0z$ are the Eyring-Powell fluid parameters with constants β_0 and δ_0.

Furthermore, Table 1 provides the properties of methanol, AA7075, and AA7072. Note that ϕ_1 and ϕ_2 denote AA7075 and AA7072 nanoparticles, respectively, where $\phi_{hnf}=\phi_1+\phi_2$. Meanwhile, the correlations of hybrid nanofluid are presented in Table 2.

Table 1. The thermophysical properties [40]

Properties	ρ(kg/m^3)	C_p(J/kgK)	k(W/mK)	σ(S/m)	Pr
Methanol	792	2545	0.2035	0.5×10^{-6}	7.38
AA7075	2810	960	173	26.77×10^{6}	
AA7072	2720	893	222	34.83×10^{6}	

Table 2. Hybrid nanofluid correlations [24]

Dynamic viscosity: $\mu_{hnf} = \dfrac{\mu_f}{(1-\phi_{hnf})^{2.5}}$
Density: $\rho_{hnf} = (1-\phi_{hnf})\rho_f + \phi_1\rho_{n1} + \phi_2\rho_{n2}$
Heat capacity: $(\rho C_p)_{hnf} = (1-\phi_{hnf})(\rho C_p)_f + \phi_1(\rho C_p)_{n1} + \phi_2(\rho C_p)_{n2}$
Thermal conductivity: $\dfrac{k_{hnf}}{k_f} = \dfrac{\frac{\phi_1 k_{n1} + \phi_2 k_{n2}}{\phi_{hnf}} + 2k_f + 2(\phi_1 k_{n1} + \phi_2 k_{n2}) - 2\phi_{hnf} k_f}{\frac{\phi_1 k_{n1} + \phi_2 k_{n2}}{\phi_{hnf}} + 2k_f - (\phi_1 k_{n1} + \phi_2 k_{n2}) + \phi_{hnf} k_f}$
Electrical conductivity: $\dfrac{\sigma_{hnf}}{\sigma_f} = \dfrac{\frac{\phi_1\sigma_{n1} + \phi_2\sigma_{n2}}{\phi_{hnf}} + 2\sigma_f + 2(\phi_1\sigma_{n1} + \phi_2\sigma_{n2}) - 2\phi_{hnf}\sigma_f}{\frac{\phi_1\sigma_{n1} + \phi_2\sigma_{n2}}{\phi_{hnf}} + 2\sigma_f - (\phi_1\sigma_{n1} + \phi_2\sigma_{n2}) + \phi_{hnf}\sigma_f}$

The similarity variables are [16]:

$$u = -\frac{caf(\eta)}{\sqrt{\eta}}, \quad w = 2czf'(\eta), \quad \theta(\eta) = \frac{T - T_\infty}{T_w - T_\infty}, \quad \eta = \left(\frac{r}{a}\right)^2 \tag{5}$$

which satisfy the continuity equation (1). Then, we have

$$\left(\frac{\mu_{hnf}}{\mu_f} + \beta_1\right)(\eta f''' + f'') - \frac{4}{Re}\beta_1\delta_1\left(\eta^2 f''^2 f''' + \frac{1}{3}\eta f''^3\right)$$

$$+ \frac{\rho_{hnf}}{\rho_f} Re(ff'' - f'^2 + 1) - \frac{\sigma_{hnf}}{\sigma_f} M(f' - 1) = 0, \tag{6}$$

$$\frac{1}{Pr}\frac{1}{(\rho C_p)_{hnf}/(\rho C_p)_f}\left(\frac{k_{hnf}}{k_f}+\frac{4}{3}R\right)(\eta\theta''+\theta')+Re(f\theta'-2f'\theta)$$

$$+\frac{Ec}{(\rho C_p)_{hnf}/(\rho C_p)_f}\left(\left(\frac{\mu_{hnf}}{\mu_f}+\beta_1\right)\eta f''^2-\frac{4}{3Re}\beta_1\delta_1\eta^2 f''^4\right)$$

$$+\frac{\sigma_{hnf}/\sigma_f}{(\rho C_p)_{hnf}/(\rho C_p)_f}MEc(f'-1)^2=0 \tag{7}$$

subject to:

$$f(1)=0,\ f'(1)=\lambda,\ \theta(1)=1;$$

$$f'(\infty)=1,\ \theta(\infty)=0, \tag{8}$$

where $\lambda=b/c$ (stretching/shrinking parameter) with $\lambda=0$ (static cylinder), $\lambda>0$ (stretching cylinder), and $\lambda<0$ (shrinking cylinder), Reynolds number $Re=ca^2/2\nu_f$, Prandtl number $Pr=\mu_f(C_p)_f/k_f$, magnetic parameter $M=\sigma_f a^2 B_0^2/4\nu_f\rho_f$, Eckert number $Ec=4c^2/(C_p)_f T_0$, and radiation parameter $R=4\sigma^* T_\infty^3/k^* k_f$, while $\beta_1=1/\beta_0\delta_0\mu_f$ and $\delta_1=c^3/2\delta_0^2\nu_f$ are the Eyring-Powell fluid parameters.

The physical quantities are:

$$C_f=\frac{2}{\rho_f w_e^2}\left(\left(\mu_{hnf}+\frac{1}{\beta\delta}\right)\frac{\partial w}{\partial r}-\frac{1}{6\beta\delta^3}\left(\frac{\partial w}{\partial r}\right)^3\right)_{r=a},$$

$$Nu=-\frac{a}{k_f(T_w-T_\infty)}\left(k_{hnf}+\frac{16\sigma^* T_\infty^3}{3k^*}\right)\left(\frac{\partial T}{\partial r}\right)_{r=a}. \tag{9}$$

Thus

$$CFR=\left(\frac{Rez}{a}\right)C_f=\left(\frac{\mu_{hnf}}{\mu_f}+\beta_1\right)f''(1)-\frac{8}{3Re}\beta_1\delta_1 f''(1)^3,$$

$$NUR = Nu = -2\left(\frac{k_{hnf}}{k_f} + \frac{4}{3}R\right)\theta'(1), \tag{10}$$

where *CFR* and *NUR* denote the skin friction and the Nusselt number coefficients.

3. Results and Discussion

The solutions to equations (6)-(8) are computed using the bvp4c solver. According to Shampine et al. [41], the bvp4c solver is designed to solve boundary value problems (BVPs) with high accuracy using adaptive mesh refinement and collocation methods. However, the accuracy of the solution is highly sensitive to the choice of initial guesses for the boundary conditions. When the problem is well-posed and the initial conditions are properly specified, bvp4c can produce accurate and reliable results. If the method struggles with convergence or the initial guesses are inadequate, then inaccuracies may occur. The influence of various physical parameters is subsequently examined and presented in both graphical and tabular forms. To validate the reliability of the model, comparisons of $f''(1)$ are provided for different values of Reynolds number (*Re*), as detailed in Table 3. In limiting cases, our results agree with those reported by Wang [16], affirming the accuracy, validity, and precision of the numerical findings in this study.

Table 3. Values of $f''(1)$ for *Re* when $\beta_1 = \delta_1 = \lambda = M = \phi_1 = \phi_2 = 0$

Re	Present results	Wang [16]
0.2	0.786042	0.78605
1	1.484183	1.484185
10	4.162920	4.16292

The effect of the Eyring-Powell fluid parameter β_1 is to increase the values of skin friction (*CFR*) and the Nusselt number (*NUR*) coefficients as shown in Figures 2 and 3. From a physical perspective, these behaviors result from a decrease in fluid viscosity, leading to a reduction in the thickness of both the momentum and thermal layers. These led to an

augment in the velocity and temperature gradients for a larger value of β_1. Therefore, the values of *CFR* and *NUR* are boosted with β_1. In addition, the existence of the dual solutions is extended with β_1, where the solutions are terminated at $\lambda_{c1} = -1.63869\,(\beta_1 = 0)$, $\lambda_{c2} = -1.65618\,(\beta_1 = 0.1)$, and $\lambda_{c3} = -1.67264\,(\beta_1 = 0.2)$.

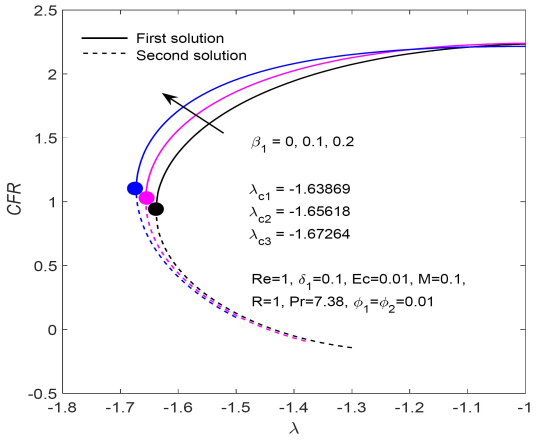

Figure 2. *CFR* versus λ and β_1.

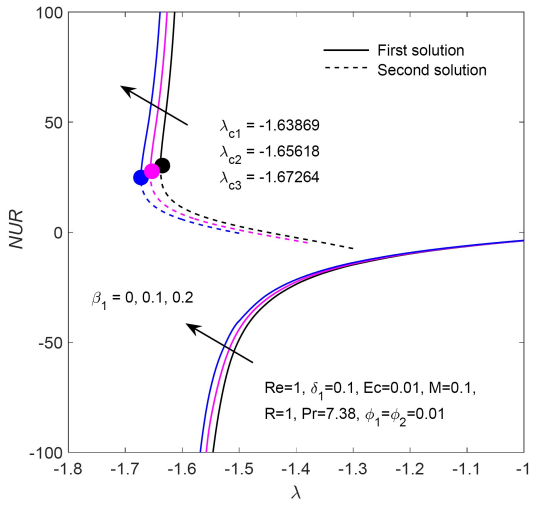

Figure 3. *NUR* versus λ and β_1.

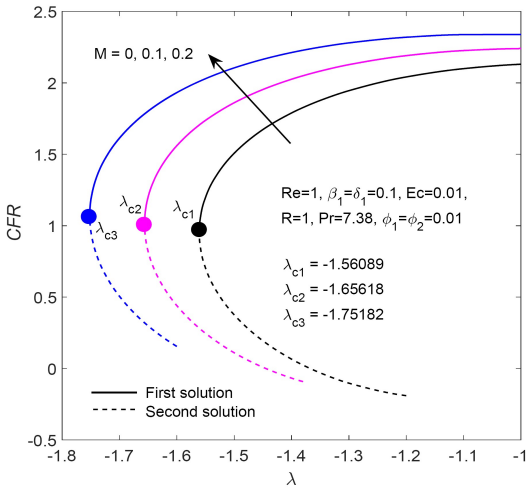

Figure 4. *CFR* versus λ and *M*.

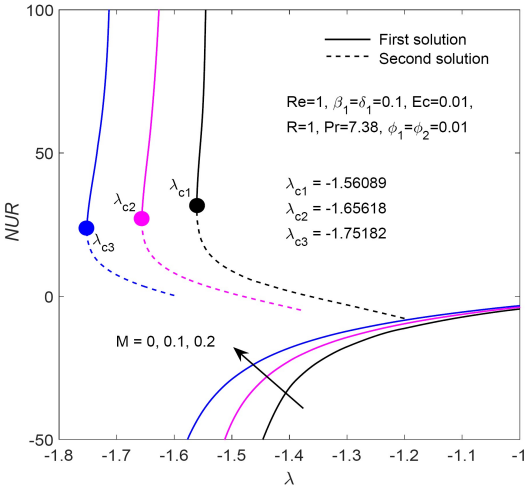

Figure 5. *NUR* versus λ and *M*.

Additionally, Figures 4 and 5 illustrate how shrinking (λ) and magnetic (M) parameters influence *CFR* and *NUR*. It is noteworthy that dual solutions emerge for specific λ values as *M* increases, with critical points occurring at $\lambda_{c1} = -1.56089\,(M = 0)$, $\lambda_{c2} = -1.65618\,(M = 0.1)$, and $\lambda_{c3} = -1.75182\,(M = 0.2)$. Moreover, *CFR* and *NUR* values are enhanced with the introduction of *M*.

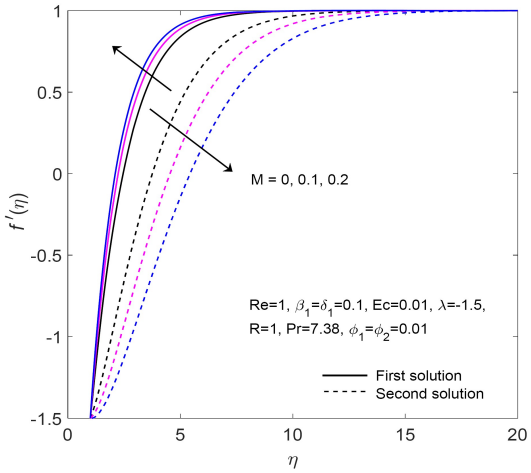

Figure 6. $f'(\eta)$ versus M.

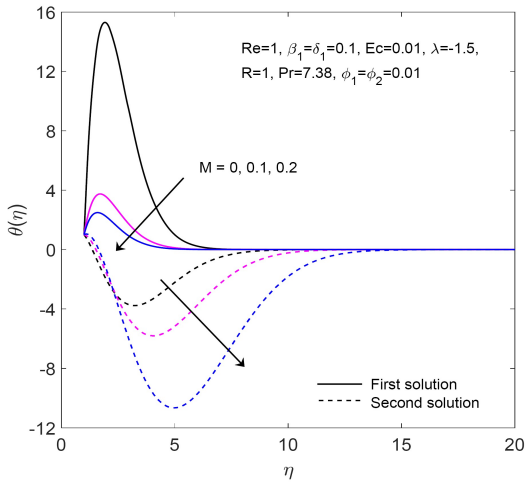

Figure 7. $\theta(\eta)$ versus M.

In Figures 6 and 7, velocity $f'(\eta)$ and temperature $\theta(\eta)$ profiles are shown for different M values. Far field boundary conditions were asymptotically met. The presence of a magnetic field can alter the fluid's flow behavior by influencing its velocity and temperature distribution due to Lorentz force. MHD effects can enhance or suppress the fluid flow, depending on the magnetic field's strength and orientation. In this study,

increasing magnetic strength reduces momentum and thermal boundary layer thicknesses. The growing Lorentz force from the magnetic field hinders fluid motion more effectively, raising the skin friction coefficient as the flow contracts. Additionally, the magnetic parameter boosts thermal conduction rates, aiding fluid movement and guiding hot particles towards the plate.

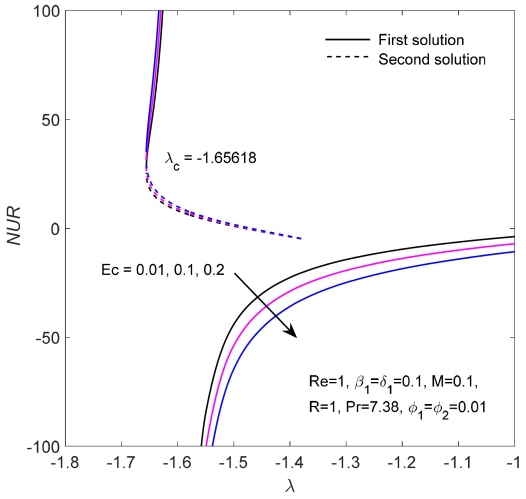

Figure 8. *NUR* versus λ and *Ec*.

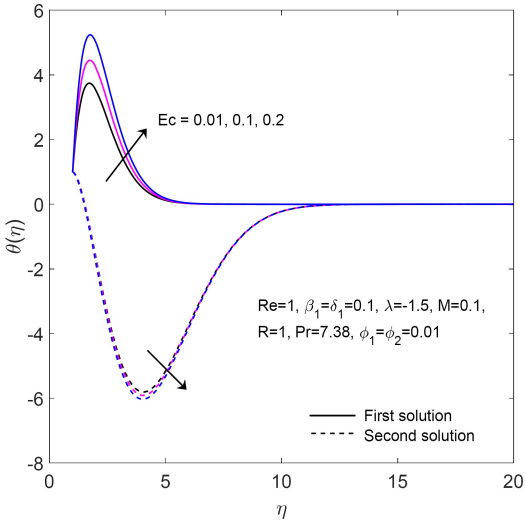

Figure 9. $\theta(\eta)$ versus *Ec*.

Figure 8 illustrates the impact of the Eckert number (*Ec*) on the *NUR*. Physically, the Eckert number represents the ratio of kinetic energy transport to the enthalpy difference across the boundary layer. This heat affects the temperature distribution and can influence the overall flow behavior by modifying the viscosity and thermal conductivity of the hybrid nanofluid. By mitigating fluid stress, Eckert numbers facilitate the conversion of kinetic energy into internal energy, thereby diminishing the influence of enthalpy differences, particularly under high kinetic energy conditions. Consequently, as depicted in Figure 9, the thickness of the thermal boundary layer increases, indicating a rise in fluid temperature. This reduction in the Eckert number (*Ec*) results in a decreased temperature gradient and consequently reduces heat transfer. A higher Eckert number, which signifies greater viscous dissipation, can elevate the fluid temperature, potentially leading to thermal inefficiency in the system by reducing the overall heat transfer.

4. Conclusions

The study examined an Eyring-Powell fluid flow incorporating viscous dissipation, MHD, and Joule heating effects. Additionally, a hybrid nanofluid was formulated by dispersing AA7075-AA7072 nanoparticles in methanol. The cylinder surface was assumed to move linearly towards the stagnation region. Dual solutions were found in the shrinking region, where the solution domain elongates with increasing magnetic and Eyring-Powell fluid parameters. These parameters were observed to enhance both heat transfer rate and skin friction. However, an increase in the Eckert number was noted to decrease heat transfer. By leveraging the effects of these physical parameters, engineers can design more efficient and effective fluid flow systems across various applications such as in heat exchangers, aerospace systems, power engineering, food processing, and petroleum production. In these contexts, industries can achieve greater efficiency, sustainability, and performance, resulting in cost savings and improved product reliability.

Acknowledgements

We appreciate the financial supports from Universiti Teknikal Malaysia Melaka (JURNAL/2022/FTKIP/Q00088).

The authors thank the anonymous referees for their valuable suggestions and constructive criticisms which improved the presentation of the paper.

References

[1] T. Hayat, Z. Hussain, M. Farooq and A. Alsaedi, Magnetohydrodynamic flow of Powell-Eyring fluid by a stretching cylinder with Newtonian heating, Thermal Science 22 (2018), 371-382.

[2] R. E. Powell and H. Eyring, Mechanisms for the relaxation theory of viscosity, Nature 154 (1944), 427-428.

[3] H. K. Yoon and A. J. Ghajar, A note on the Powell-Eyring fluid model, International Communications in Heat and Mass Transfer 14 (1987), 381-390.

[4] A. Riaz, R. Ellahi, M. M. Bhatti and M. Marin, Study of heat and mass transfer in the Eyring-Powell model of fluid propagating peristaltically through a rectangular compliant channel, Heat Transfer Research 50 (2019), 1539-1560.

[5] M. M. Bhatti, T. Abbas, M. M. Rashidi, M. Ali and Z. Yang, Entropy generation on MHD Eyring-Powell nanofluid through a permeable stretching surface, Entropy 18 (2016), 224.

[6] A. Riaz, R. Ellahi and S. M. Sait, Role of hybrid nanoparticles in thermal performance of peristaltic flow of Eyring-Powell fluid model, Journal of Thermal Analysis and Calorimetry 143 (2021), 1021-1035.

[7] A. V. Roşca and I. Pop, Flow and heat transfer of Powell-Eyring fluid over a shrinking surface in a parallel free stream, International Journal of Heat and Mass Transfer 71 (2014), 321-327.

[8] M. Jalil, S. Asghar and S. M. Imran, Self similar solutions for the flow and heat transfer of Powell-Eyring fluid over a moving surface in a parallel free stream, International Journal of Heat and Mass Transfer 65 (2013), 73-79.

[9] A. Ara, N. A. Khan, H. Khan and F. Sultan, Radiation effect on boundary layer flow of an Eyring-Powell fluid over an exponentially shrinking sheet, Ain Shams Engineering Journal 5 (2014), 1337-1342.

[10] N. S. Akbar, A. Ebaid and Z. H. Khan, Numerical analysis of magnetic field effects on Eyring-Powell fluid flow towards a stretching sheet, Journal of Magnetism and Magnetic Materials 382 (2015), 355-358.

[11] E. O. Fatunmbi and A. T. Adeosun, Nonlinear radiative Eyring-Powell nanofluid flow along a vertical Riga plate with exponential varying viscosity and chemical reaction, International Communications in Heat and Mass Transfer 119 (2020), 104913.

[12] T. M. Agbaje, S. Mondal, S. S. Motsa and P. Sibanda, A numerical study of unsteady non-Newtonian Powell-Eyring nanofluid flow over a shrinking sheet with heat generation and thermal radiation, Alexandria Engineering Journal 56 (2017), 81-91.

[13] A. Aljabali, A. R. M. Kasim, N. S. Arifin, S. Mohamad Isa and N. A. N. Ariffin, Analysis of convective transport of temperature-dependent viscosity for non-Newtonian Eyring-Powell fluid: a numerical approach, Computers, Materials and Continua 66 (2021), 675-689.

[14] I. Waini, A. Ishak and I. Pop, Eyring-Powell fluid flow past a shrinking sheet: Effect of magnetohydrodynamic (MHD) and Joule heating, Journal of Advanced Research in Fluid Mechanics and Thermal Sciences 116(1) (2024), 64-77.

[15] C. Wang, Axisymmetric stagnation flow on a cylinder, Quarterly of Applied Mathematics 32 (1974), 207-213.

[16] C. Y. Wang, Fluid flow due to a stretching cylinder, Phys. Fluids 31 (1988), 466.

[17] A. Ishak, R. Nazar and I. Pop, Uniform suction/blowing effect on flow and heat transfer due to a stretching cylinder, Applied Mathematical Modelling 32 (2008), 2059-2066.

[18] I. S. Awaludin, R. Ahmad and A. Ishak, On the stability of the flow over a shrinking cylinder with prescribed surface heat flux, Propulsion and Power Research 9(2) (2020), 181-187.

[19] N. C. Roy and A. Akter, Dual solutions of mixed convective hybrid nanofluid flow over a shrinking cylinder placed in a porous medium, Heliyon 9(11) (2023), e22166.

[20] S. U. S. Choi and J. A. Eastman, Enhancing thermal conductivity of fluids with nanoparticles, Proceedings of the 1995 ASME International Mechanical Engineering Congress and Exposition, FED 231/MD, Vol. 66, 1995, pp. 99-105.

[21] B. C. Pak and Young I. Cho, Hydrodynamic and heat transfer study of dispersed fluids with submicron metallic oxide, Experimental Heat Transfer 11 (1998), 151-170.

[22] C. J. Ho, W. K. Liu, Y. S. Chang and C. C. Lin, Natural convection heat transfer of alumina-water nanofluid in vertical square enclosures: an experimental study, International Journal of Thermal Sciences 49 (2010), 1345-1353.

[23] B. Takabi and S. Salehi, Augmentation of the heat transfer performance of a sinusoidal corrugated enclosure by employing hybrid nanofluid, Advances in Mechanical Engineering 6 (2014), 147059.

[24] U. Khan, A. Zaib, A. Ishak, E.-S. M. Sherif, I. Waini, Y.-M. Chu and I. Pop, Radiative mixed convective flow induced by hybrid nanofluid over a porous vertical cylinder in a porous media with irregular heat sink/source, Case Studies in Thermal Engineering 30 (2022), 101711.

[25] N. S. Khashi'ie, I. Waini, S. M. Zokri, A. R. M. Kasim, N. M. Arifin and I. Pop, Stagnation point flow of a second grade hybrid nanofluid induced by a Riga plate, International Journal of Numerical Methods for Heat and Fluid Flow 32 (2021), 2221-2239.

[26] B. Mahanthesh, S. A. Shehzad, T. Ambreen and S. U. Khan, Significance of Joule heating and viscous heating on heat transport of MoS2-Ag hybrid nanofluid past an isothermal wedge, Journal of Thermal Analysis and Calorimetry 143 (2021), 1221-1229.

[27] M. Ghalambaz, N. C. Rosca, A. V. Rosca and I. Pop, Mixed convection and stability analysis of stagnation-point boundary layer flow and heat transfer of hybrid nanofluids over a vertical plate, International Journal of Numerical Methods for Heat and Fluid Flow 30 (2020), 3737-3754.

[28] I. Waini, A. Ishak and I. Pop, Hybrid nanofluid flow on a shrinking cylinder with prescribed surface heat flux, International Journal of Numerical Methods for Heat and Fluid Flow 31 (2021), 1987-2004.

[29] I. Waini, A. Ishak and I. Pop, Hybrid nanofluid flow over a permeable non-isothermal shrinking surface, Mathematics 9 (2021), 538.

[30] A. Mokhefi and E. R. di Schio, Effect of a magnetic field on the Couette forced convection of a Buongiorno's nanofluid over an embedded cavity, JP Journal of Heat and Mass Transfer 30 (2022), 89-104.

[31] A. K. Pati, A. Misra, S. K. Mishra, S. Mishra, R. Sahu and S. Panda, Computational modelling of heat and mass transfer optimization in copper water nanofluid flow with nanoparticle ionization, JP Journal of Heat and Mass Transfer 31 (2023), 1-18.

[32] N. A. Rahman, N. S. Khashi'ie, K. B. Hamzah, N. A. Zainal, I. Waini and I. Pop, Axisymmetric hybrid nanofluid flow over a radially shrinking disk with heat generation and magnetic field effects, JP Journal of Heat and Mass Transfer 37(3) (2024), 365-375.

[33] A. Wakif, A. Chamkha, T. Thumma, I. L. Animasaun and R. Sehaqui, Thermal radiation and surface roughness effects on the thermo-magneto-hydrodynamic stability of alumina-copper oxide hybrid nanofluids utilizing the generalized Buongiorno's nanofluid model, Journal of Thermal Analysis and Calorimetry 143 (2021), 1201-1220

[34] H. Waqas, U. Farooq, R. Naseem, S. Hussain and M. Alghamdi, Impact of MHD radiative flow of hybrid nanofluid over a rotating disk, Case Studies in Thermal Engineering 26 (2021), 101015.

[35] S. Rosseland, Astrophysik und atom-theoretische Grundlagen, Springer-Verlag, Berlin, 1931.

[36] M. Rooman, M. A. Jan, Z. Shah, N. Vrinceanu, S. Ferrándiz Bou, S. Iqbal and W. Deebani, Entropy optimization on axisymmetric Darcy-Forchheimer Powell-Eyring nanofluid over a horizontally stretching cylinder with viscous dissipation effect, Coatings 12 (2022), 749.

[37] H. A. Ogunseye, Y. O. Tijani and P. Sibanda, Entropy generation in an unsteady Eyring-Powell hybrid nanofluid flow over a permeable surface: a Lie group analysis, Heat Transfer 49 (2020), 3374-3390.

[38] I. Waini, A. Ishak and I. Pop, Hybrid nanofluid flow towards a stagnation point on a stretching/shrinking cylinder, Scientific Reports 10 (2020), 9296.

[39] S. S. Ghadikolaei, K. Hosseinzadeh and D. D. Ganji, Investigation on magneto Eyring-Powell nanofluid flow over inclined stretching cylinder with nonlinear thermal radiation and Joule heating effect, World Journal of Engineering 16 (2019), 51-63.

[40] I. Tlili, H. A. Nabwey, G. P. Ashwinkumar and N. Sandeep, 3-D magnetohydrodynamic AA7072-AA7075/methanol hybrid nanofluid flow above an uneven thickness surface with slip effect, Scientific Reports 10 (2020), 1-13.

[41] L. F. Shampine, I. Gladwell and S. Thompson, Solving ODEs with MATLAB, Cambridge University Press, Cambridge, 2003.